Appl. Phys. A 85, 387–397 (2006)
DOI: 10.1007/s00339-006-3691-0

Applied Physics A
Materials Science & Processing

W.G. SCHMIDT[1,✉]
K. SEINO[2]
M. PREUSS[2]
A. HERMANN[3]
F. ORTMANN[2]
F. BECHSTEDT[2]

Organic molecule adsorption on solid surfaces: chemical bonding, mutual polarisation and dispersion interaction

[1] Theoretische Physik, Universität Paderborn, 33095 Paderborn, Germany
[2] Institut für Festköpertheorie und -optik, Friedrich-Schiller-Universität Jena, Max-Wien-Platz 1, 07743 Jena, Germany
[3] Institute of Fundamental Sciences, Massey University, Auckland, New Zealand

Received: 17 March 2006/Accepted: 9 August 2006
Published online: 16 September 2006 •

ABSTRACT We discuss some of the most relevant bonding scenarios for the adsorption of organic molecules on solid surfaces from the perspective of first-principles calculations. The adsorption of uracil and phenanthrenequinone on Si(001) and the adsorption of adenine on Cu(110) and graphite(0001) surfaces serve as prototypical examples to highlight relevant molecule–substrate interactions and their consequences for the properties of the adsystem. Covalent bonds formed during organic reactions with semiconductor surfaces significantly modify the structural and electronic properties of both the adsorbed molecules and the substrate. Organic molecule adsorption on metals may be driven by mutual polarisation that leads to substantial charge transfer and rehybridisation, despite small adsorption energies. Subtle effects related to the lowering of the kinetic energy of the valence electrons as well as dispersion forces, finally, govern the interaction between the organic molecules and chemically inert substrates such as graphite.

PACS 68.35.Md; 68.43.Bc; 68.43.-h; 73.20.-r; 82.39.Pj

1 Introduction

Organic molecules are very promising building blocks for electronic devices due to the possibility of tailoring molecules with particular properties, the tunability of their characteristics and the efficiency and flexibility of deposition methods. Their functionality with respect to molecular electronics [1], nanodevices [2] and molecular recognition [3] has been intensively investigated. For some years already, molecular materials have been used in solar cells, gas sensors, heterojunctions and ultra-fast optical switches. Because they have typically dimensions of a few nanometres, molecules are the ultimate limit of electronic devices.

Self-organisation of organic molecules appears as one of the most promising approaches to the further miniaturisation of electronic devices. This so-called bottom-up approach contrasts with the exponentially increasing fabrication costs of further down-scaling the lithographic processes in the top-down approach for device manufacturing. The latter approach already has led to atomic dimensions (the gate oxide thickness of the presently produced transistors of the 65-nm generation amounts to only 1.2 nm, i.e. about 4–5 atomic SiO_2 layers) and is bound to lead soon to fundamental physical limits. The rich variety of living structures that are all based on different combinations of a few molecular building blocks, i.e. amino acids, proves the usefulness and robustness of the bottom-up approach for producing complex structures. However, we are only beginning to understand how the mechanisms of molecular recognition and self-assembly could be exploited for actual device production.

In order to investigate the molecular self-organisation, suitable model systems need to be found that allow us to study the molecular interactions reproducibly and with high accuracy. Surface adsorbed molecules are an obvious choice. They are accessible to sophisticated surface analysis tools such as scanning tunnelling microscopy (STM) as well as electron diffraction techniques, infrared and other optical spectroscopies. However, suitable substrates must be chosen that ensure that the molecule–molecule interactions are not completely masked by the interactions between the substrate and the molecules. In this context, metal substrates or graphite are often used as static checkerboards for the molecules [4, 5]. In particular in the latter case, the substrate-induced perturbations of the molecular properties are minimal and the molecule seems to swim freely on the substrate, as illustrated in Fig. 1 for the case of adenine adsorbed on graphite(0001) [6]. Highly ordered structures of adenine are also observed on Cu(111) [7–9] and on Cu(110) surfaces [10]. STM images show that in the latter case ordered one-dimensional molecular chains grow along the lateral $[\pm 1, 2]$ directions (given with respect to $[\bar{1}10]$ and [001]). Upon increasing the adenine coverage, the chains order into chiral domains of $\begin{pmatrix} 1 & 2 \\ 6 & 0 \end{pmatrix}$ periodicity. The interaction of homochiral adenine chains on Cu(110) with inherently chiral molecules may lead to the formation of diastereoisomers due to enantiomeric interactions [11]: while co-adsorption of S-phenylglycine leads to decorations of only those adenine chains that are oriented along the [1, 2] direction in the surface plane (see Fig. 2), the separate adsorption of R-phenylglycine on an adenine-treated Cu surface shows amino acid molecules now decorating chains aligned along $[-1, 2]$.

While metal and chemically inert surfaces are well suited for investigating such fundamental aspects of molecular

✉ Fax: +49 5251 603435, E-mail: w.g.schmidt@upb.de

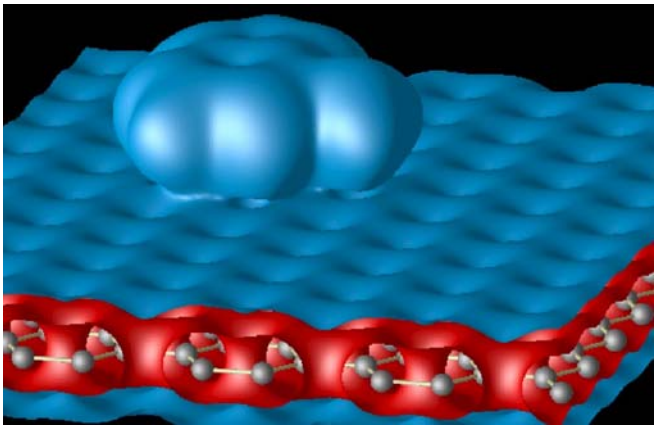

FIGURE 1 Isosurfaces of the calculated total valence charge density of adenine adsorbed on graphite(0001). The positions of the carbon atoms in the uppermost graphene sheet are indicated

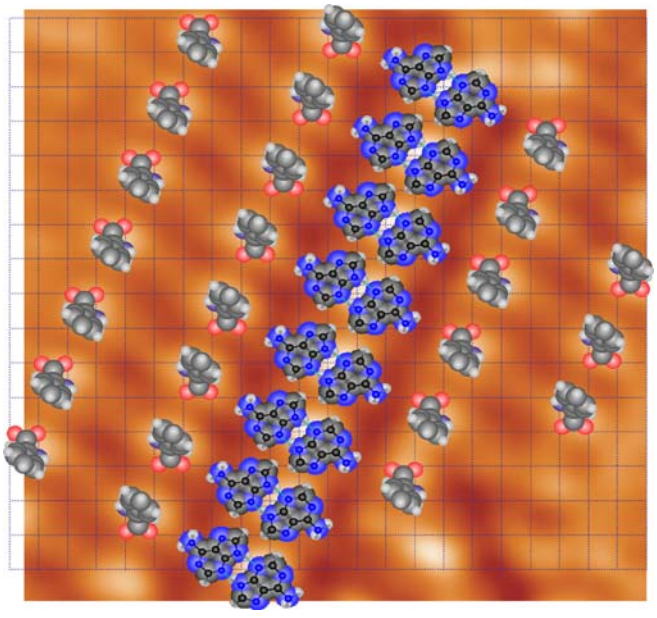

FIGURE 2 Suggested model for the arrangement of S-phenylglycine dimer rows and adenine chains on the Cu(110) surface superimposed on the measured STM image. The *grey lines* indicate the Cu surface periodicity. Data from [11]

recognition and self-assembly, organic molecule adsorption on semiconductor surfaces seems now to become more relevant for device applications. In fact, the combination of the available and highly sophisticated silicon-based integrated-circuit technology with the rich variety of chemical, electronic and optical properties that can be realised using tailor-made organic molecules is very promising for the development of new semiconductor-based devices [12, 13].

In chemistry, structural theory is an extremely useful method of classifying the enormous number of organic compounds into smaller, more tractable families. It is based on the observation that molecules with similar arrangements of atoms will react similarly. These atomic arrangements are known as functional groups. Polyfunctional organic molecules can react with solid surfaces in a variety of ways, which opens the possibility of purposeful tuning of the surface properties. The adsorption of polyfunctional groups on solid surfaces can also be used to form an ordered array of functional groups available for further reactions [14, 15].

The deoxyribose nucleic acid (DNA) bases adenine, guanine, cytosine and thymine as well as uracil are polyfunctional molecules that are particularly amenable to the synthesis of complex molecular structures, due to their Watson–Crick complementarity. In this brief review, we use the adsorption of uracil and phenanthrenequinone on Si(001) as well as the adsorption of adenine on Cu(110) and graphite(0001) surfaces as prototypical model systems to highlight important aspects of organic molecule adsorption on solid surfaces.

2 Adsorption on semiconductor surfaces

Some functional groups relevant for molecular adsorption on semiconductor surfaces are shown in Fig. 3. They are separated into two categories, see also [16]: the bonding functional groups include alkanes, alkenes and alkynes. Each of these functional groups have all of their valence electrons paired in bonds between neighbouring atoms. Alcohols, amines, carbonyls and nitriles, in contrast, contain non-bonding valence electrons that are not paired with an electron from an adjacent atom. These non-bonding electrons are spin coupled into a single non-bonding orbital also known as a lone pair. This division of organic molecules allows for a rough classification of organic chemistry at the semiconductor surface: molecules with bonding functional groups tend to form pericyclic surface products. The $[2+2]$ cycloaddition reaction of cyclopentene with Si(001) is a well-investigated example [14, 17, 18]. Molecules with non-bonding groups, on the other hand, have a significant cloud of electronic charge that can be donated during electrophilic/nucleophilic reactions, e.g. by forming a dative bond with the 'down' Si(001) surface dimer atom. Often this is the precursor for a subsequent proton transfer. The adsorption of pyrrole [19] or butanediol on Si(001) [20] are examples for the latter class of reactions. However, there are examples that are not so easily categorised. Phenanthrenequinone, for example, has two carbonyl groups that allow for the formation of a $[4+2]$ cycloaddition product with the Si(001) surface dimer [21, 22]. However, the donation of the O lone-pair electrons into the empty p_z orbital of the Si down dimer atom is the probable precursor state.

The adsorption in a weakly bound precursor state by dint of lone-pair donation followed by a proton transfer is reminiscent of water adsorption on Si(001) [23, 24]. Upon heating the substrate to around 600 K, the oxygen of the surface bonded hydroxyl group can insert into the silicon to form a Si–O–Si structure. The pathway to oxidation, however, consists of multiple activation barriers [25]. Similarly, the adsorption of organic molecules on the surface may occur in steps, where the formation of the final structure will depend on the preparation conditions. Unlike the relatively simple case of water, however, the complexity of organic molecules allows for exploiting the activation barriers to tune the surface electronic and optical properties. This has been investigated by Seino et al. for the case of uracil adsorption on Si(001) [26, 27] using density functional theory (DFT) calculations within the generalised gradient approximation (GGA).

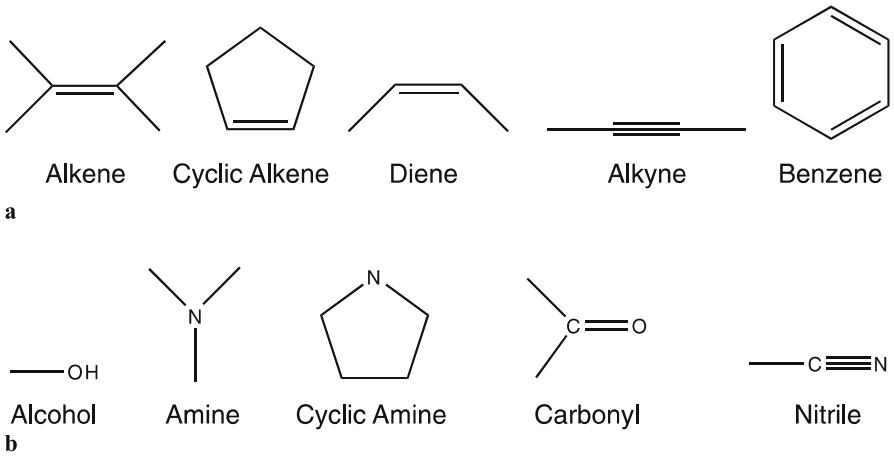

FIGURE 3 Several (**a**) bonding and (**b**) non-bonding functional groups relevant to molecular adsorption on semiconductor surfaces

The adsorption of uracil on Si(001), investigated experimentally by STM and high-resolution electron energy-loss spectroscopy [28], leads to what can be considered a prototypical interface between a polyfunctional molecule and a semiconductor surface. The (001) surface of silicon is the starting point for the fabrication of most microelectronic devices. Uracil ($C_4H_4N_2O_2$) is a small molecule featuring one C=C double bond, two N–H and two carbonyl groups and may thus bond to the surface in various ways. In addition, its tautomerism and electrostatic effects have been found to be important for the interface formation [28, 29].

From previous total-energy calculations [29] in conjunction with experimental work [28] it was concluded that uracil adsorption on Si(001) is governed by the carbonyl groups and is likely to result in dimer bridging configurations such as shown in Fig. 4. Starting from a dative-bonded configuration, where uracil is attached to the electron-poor 'down' Si dimer atom via one carbonyl group, a relatively low energy barrier of about 0.3 eV needs to be overcome for hydrogen dissociation, molecular rotation around the surface normal and tilting towards the neighbouring Si dimer [29]. This leads to a structure where uracil binds partially dative, i.e. with one covalent and one dative bond to the Si surface, bridging two Si dimer rows (Fig. 4a). An energy barrier larger than 1 eV needs to be overcome for oxygen insertion into Si dimers, leading to the covalently bonded interface configuration shown in Fig. 4b. The formation of this structure therefore requires annealing at elevated temperatures. The calculated adsorption energies of the partially dative (D) and covalently bonded interface models (C) amount to 2.77 and 5.27 eV, respectively. The dative bond in the structure D occurs between the electron-rich uracil carbonyl group and the electron-poor atom of the clean

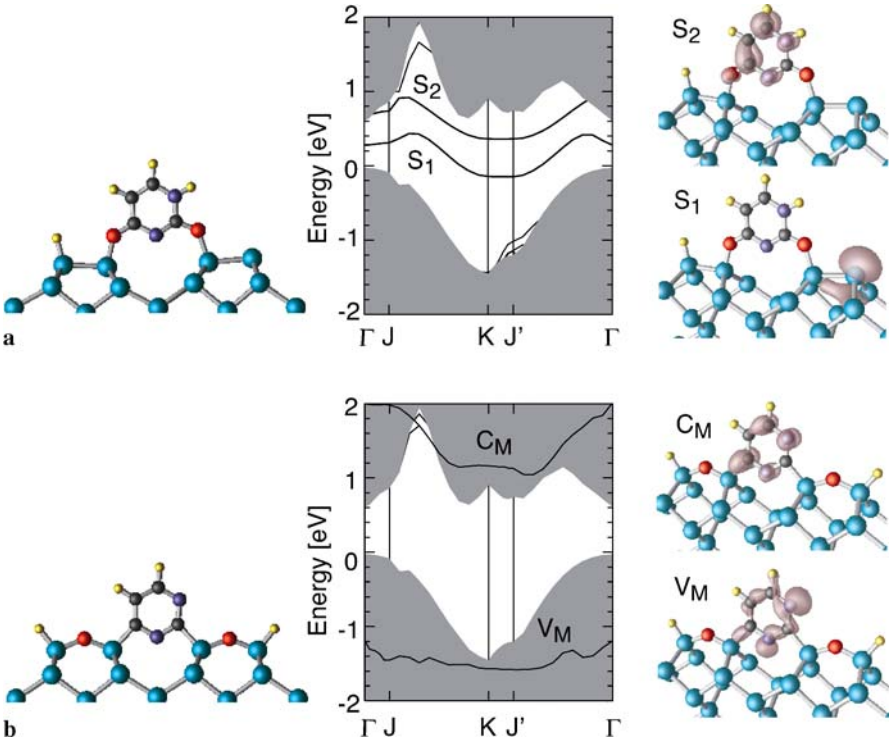

FIGURE 4 *Left*: suggested dative-bonded (**a**) and covalently bonded (**b**) adsorption configurations for uracil/Si(001). *Grey*, *purple*, *blue*, *red* and *yellow symbols* indicate C, N, Si, O and H atoms, respectively. *Middle*: surface band structures for the two interface models. *Grey regions* indicate the projected Si bulk bands. *Right*: the orbital character of specific states is indicated by isosurfaces for 0.05 $Å^{-3}$. Data from [27]

Si dimer. It is about 0.1 Å longer than the corresponding covalent Si–O bond [29].

The surface band structures calculated for the structural models discussed above can be clear-cut classified. Model C, where exclusively covalent bonds occur, leads to a perfect surface passivation, as shown in Fig. 4b. The Si-dimer-related D_{up} and D_{down} bands characteristic for the clean Si(001) surface [30] disappear, due to the formation of Si–O and Si–C σ bonds, which lie energetically below the bulk Si valence-band edge. The corresponding antibonding σ^* combinations occur above the Si conduction-band edge. No molecular electronic states exist in the energy region of the Si fundamental gap. The highest occupied and lowest unoccupied molecule states, V_{M} and C_{M}, respectively, occur below and above the bulk valence and conduction-band edges.

The situation is very different for the partially dative-bonded model D. We find two prominent surface states, S_1 and S_2, in the energy region of the Si bulk band gap (cf. Fig. 4a). At least within the DFT-GGA, which usually suffers from an underestimation of excitation energies [31], these two states give rise to a semimetallic band structure and pin the Fermi level. The orbital character of S_1 is very similar to the surface state localised at the 'up' dimer atom of the clean Si(001) surface [30]. The dispersion of S_1 perpendicular to the dimer row direction is very small, whereas a large dispersion is calculated for the direction parallel to the dimer rows. The S_2 state is uracil derived. It is mainly formed by non-bonding carbon and nitrogen p orbitals. Again, due to the interaction between neighbouring molecules, a strong dispersion for the direction parallel to the dimer rows is predicted. The electronic structure calculated for the D interface seems to indicate one-dimensional metallic character, i.e. conductivity along the dimer row direction. From STM it is known that the uracil molecules indeed form lines parallel to the Si dimer rows [28]. There are, however, two possible orientations: the molecules may either arrange in a (4×1) translational symmetry, or every second molecule can be rotated by 180°, forming a (4×2) surface. The calculated total energies [27] show that the latter case is energetically slightly preferred, by tenths of an eV. The alternating arrangement of the uracil molecules (and, consequently, hydrogen atoms) leads to a much reduced energy dispersion of the S_1 and S_2 surface states and thus to the opening of a small energy gap.

The ionisation energy (or photoelectric threshold) of a surface is given by the energy difference between the vacuum level and the valence-band maximum. It can be calculated by combining bulk and surface calculations [32, 33]. The calculations predict a drastic reduction of the ionisation energy by more than two eV for the D interface model. After the formation of covalent bonds, i.e. for the structure C, the ionisation energy becomes closer to the value of the clean surface. Clean Si(001) surfaces experience a reduction of the ionisation energy by about 0.35 eV upon exposure to atomic hydrogen. This is explained by the hydrogen-induced conversion of tilted into untilted dimers, neutralising the electric double layer formed by filled and empty Si dimer atom dangling bonds [34]. The effect found here is much stronger and not correlated to the tilting of the Si surface dimers. In order to explore the uracil-induced changes of the electronic structure in more detail, the charge difference

$$\Delta\varrho(\boldsymbol{r}) = \varrho_{\mathrm{U/Si}}(\boldsymbol{r}) - \varrho_{\mathrm{Si}}(\boldsymbol{r}) - \varrho_{\mathrm{U}}(\boldsymbol{r})\,, \tag{1}$$

was computed, where $\varrho_{\mathrm{U/Si}}$ is the (negative) electron density calculated for the slab describing the uracil-adsorbed Si(001) surface, ϱ_{Si} is that for the clean relaxed Si(001) surface and ϱ_{U} is that for a gas-phase uracil molecule in the (possibly dissociated) configuration assumed for the respective bonding geometry. The positive and negative charge differences allow us to calculate the average adsorption-induced dipole charge $Q^{\pm}$ and the dipole length projected onto the surface normal, d_z,

$$Q^{\pm} = \int\limits_{\Delta\varrho(\boldsymbol{r})\gtrless 0} \mathrm{d}\boldsymbol{r}\Delta\varrho(\boldsymbol{r})\,, \tag{2}$$

$$d_z = \frac{1}{Q^{+}} \int\limits_{\Delta\varrho(\boldsymbol{r})>0} \mathrm{d}\boldsymbol{r}\Delta\varrho(\boldsymbol{r})z - \frac{1}{Q^{-}} \int\limits_{\Delta\varrho(\boldsymbol{r})<0} \mathrm{d}\boldsymbol{r}\Delta\varrho(\boldsymbol{r})z\,. \tag{3}$$

In order to determine the charge transferred parallel to the surface normal, $Q^{\pm}_{||}$, and its separation, $d_{||}$, we start from the charge difference averaged over the surface unit cell

$$\overline{\Delta\varrho}(z) = \frac{1}{A} \int\limits_{A} \mathrm{d}x\,\mathrm{d}y\Delta\varrho(\boldsymbol{r})\,, \tag{4}$$

and proceed in analogy to (2) and (3).

The calculated values for these quantities are compiled in Table 1. Obviously, the overall uracil-induced charge transfer is rather large, with $Q^{\pm}$ values of 5–8 electrons. This is simply due to the substantial rebonding processes taking place upon molecule adsorption. For model C already about 50% of the charge transfer is due to the breaking of Si dimers. Only 1–3 electrons are transferred parallel to the surface normal, with a charge separation of 1.5–2.4 Å (cf. Table 1). These values are of similar magnitude to the ones calculated for the Cs/GaAs interface [35]. The electrons forming the bonds between uracil and the substrate originate from the substrate rather than from the molecule. There is even a slight accumulation of additional charge at the adsorbed molecule, as shown in Fig. 5 for the dative-bonded interface. This is plausible, giving the high electronegativity of carbon (2.55), nitrogen (3.04) and oxygen (3.44) compared to the one of silicon (1.9). However, the net electron transfer from the substrate towards the molecule seemingly contradicts the calculated decrease of the ionisation energy by up to 2.4 eV. Rather, an increase of the ionisation energy would be expected, such as for example found upon chlorine adsorption on semiconductor surfaces [34]. The apparent contradiction is due to the dipole moments of the uracil molecules themselves, that form the outermost layer of the adsorbate system. The uracil

	d_z	$d_{\|\|}$	$\|Q^{\pm}\|$	$\|Q^{\pm}_{\|\|}\|$	$p_z = \|Q^{\pm}\| \times d_z$	ΔI
D	−0.6	−2.4	4.8	1.3	−14.6	−2.4
C	−0.5	−1.5	7.6	2.5	−17.9	−0.5

TABLE 1 Dipole lengths d_z and $d_{||}$ (in Å), dipole charges $Q^{\pm}$ and $Q^{\pm}_{||}$ (in e), dipole moment p_z (in Debye) and changes of the ionisation energy ΔI due to uracil adsorption (in eV)

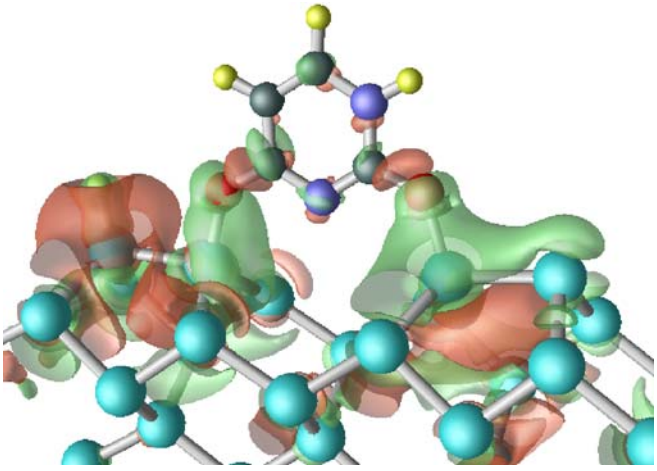

FIGURE 5 Calculated electron density differences $\Delta\varrho(\boldsymbol{r})$ for the D interface model of uracil adsorbed on Si(001). *Green* and *orange* isosurfaces for ± 0.03 Å^{-3} indicate electron gain and loss. Data from [27]

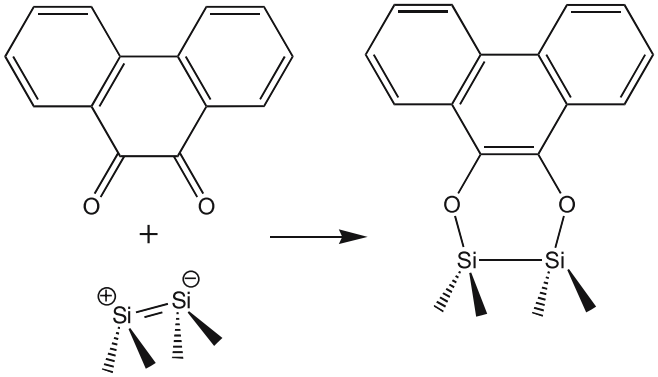

FIGURE 6 Proposed bonding mechanism for the chemisorption of 9,10-phenanthrenequinone on Si(001)

dipole moment is mainly carbonyl group related, and therefore depends strongly on the specific tautomer. For gas-phase molecules it may reach 7.5 Debye [36]. The molecular dipole points away from the carbonyl groups and thus along the surface normal in the adsorption configurations studied here.

Altogether, we find that the electronic properties of the uracil/Si(001) interface depend strongly on the details of the chemical bonding and adsorption geometry. Dative-bonded interfaces are characterised by a high density of states in the energy region of the fundamental gap and a very strong reduction of the ionisation energy. The formation of covalent bonds at the interface accompanied by a transfer of protons from the molecule to the semiconductor surface leads to an electronically passivated surface with an ionisation energy close to the value of the clean surface.

The adsorption of uracil on Si(001) is an illustrative example that highlights the impact of thin organic layers on semiconductor surface properties. However, the adsorption also strongly modifies the molecular electronic structure, even if the functional groups bonding the molecule to the substrate are well separated from the rest of the molecule. The adsorption of 9,10-phenanthrenequinone (PQ, $C_{14}O_2H_8$) on Si(001) may serve as a prototypical process of such kind. It was investigated by various experimental techniques probing structural, electronic and optical properties of the adsorbed layer [21, 37]. PQ has two highly reactive carbonyl groups that realise the bonding to the surface as well as a delocalised π electron system that remains intact upon adsorption: in the most favoured adsorption geometry PQ sits atop the Si dimer, forming a $[4+2]$-cycloaddition product [22, 38], as shown in Fig. 6.

Hacker and Hamers [21] studied the optical anisotropy of PQ adsorbed on Si(001) as a prototype for a π-conjugated overlayer system. A pronounced anisotropy was found for a photon energy of 5.2 eV and related to intramolecular π–π^* transitions. Detailed DFT-GGA calculations by Hermann et al. [38] showed, however, that this feature is rather due to adsorption-induced distortions of the substrate with contributions from both the adsorption-induced strain in the silicon lattice and the formation of Si–O bonds. The intramolecular optical transitions, instead, strongly change in magnitude and energy position upon bonding to the Si(001) surface. In order to study this effect in detail, Hermann et al. [22] considered a PQ + Si_2H_4 cluster, where PQ bonds via the carbonyl groups to a hydrogen-saturated Si dimer. In the left-hand part of Fig. 7 the energy shifts of the highest occupied (HOMO) and lowest unoccupied (LUMO) orbitals when going from the free PQ molecule to the PQ + Si_2H_4 cluster and the significant changes of the most relevant gas-phase optical transitions M2–M5 to the admolecule transitions M1–M3 are illustrated. The charge-density distributions of the orbitals involved in the transitions M1–M3 are shown in the right-hand part of Fig. 7. Upon bonding to the Si dimer, the PQ LUMO, which is mainly the C=C double bond of the carbonyl groups' C atoms, becomes populated and forms the new PQ + Si_2H_4 HOMO; the PQ's π and π^* orbitals are shifted upwards and two new Si–Si bond localised unoccupied states s_1 and s_2 show up. The transition M1 appears only due to formation of the new HOMO, the transitions M2 and M3 are shifted in energy and M4 and M5 disappear by losing almost all of their oscillator strength. Although spatially decoupled, the interaction between the carbonyl groups and the molecular π-electron system leads to strongly altered electronic and optical properties after adsorption on the substrate. The occurrence of strong changes in the PQ molecular electronic structure has recently been confirmed by time-dependent density functional theory [39].

The examples discussed above highlight the strong modifications of both the semiconductor and the molecular electronic structure due to the chemisorption. Results obtained for different adsorption configurations of the same molecular species on Si suggest the tailoring of surface electronic properties by means of choosing suitable preparation conditions, such as temperature, or by chemically protecting or activating specific molecular functional groups, thus controlling the molecular bonding and orientation with respect to the substrate. However, the changes of the molecular properties upon attachment to the surface may be considerable.

3 Adsorption on metal surfaces

Similarly to the case of organic molecule adsorption on semiconductors, the interaction of simple unsaturated hydrocarbons such as ethylene and benzene with metal surfaces has been explained in terms of covalent-bond for-

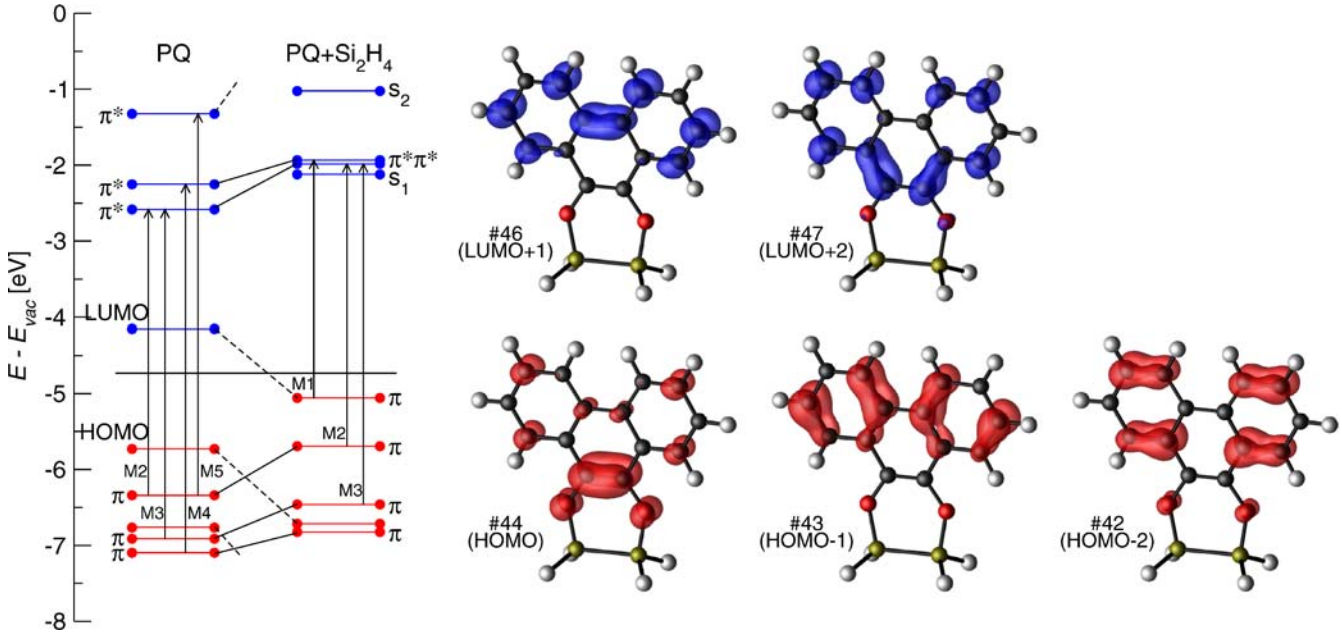

FIGURE 7 *Left*: shift of PQ orbitals and intramolecular transitions upon binding to Si_2H_4 cluster. *Right*: charge-density isosurface plots of occupied and unoccupied orbitals involved in transitions M1–M3. Data from [22]

mation. The description of bonding in these systems was originally developed by Dewar, Chatt and Duncanson (DCD model) [40, 41] and views the interaction in terms of a donation of charge from the highest occupied π orbital into the metal and a subsequent back-donation from filled metal states into the lowest unoccupied π^* orbital. An alternative description of bonding – yielding the same final charge distribution as predicted by the DCD model – is given by the 'spin-uncoupling' mechanism [42], where the bonding is described as a bond preparation through excitation of π electrons into the molecular π^* orbital, producing the molecular state that can bond to the surface. The advantage of the latter description is that it provides an estimate of the energy cost of the rehybridisation required for adsorption and thus an intuitive approach to the activation barrier. The spin-uncoupling or DCD models have been shown to describe the adsorption of a number of small unsaturated hydrocarbons fairly well [43]. The interaction between saturated hydrocarbons and metal surfaces is less well understood. Wöll et al. analysed in detail the bonding of cyclopropane (C_3H_6) on Cu(111) [44]. While essentially no bonding was found on the Hartree–Fock level of theory, a clear minimum of the potential energy curve was obtained using Møller–Plesset perturbation theory to second order (MP2). This indicates the importance of dispersion-type interactions. Also, some back-donation of charge from occupied metal orbitals to empty C_3H_6 states of Rydberg character was noticed. More recent MP2 calculations [45] on cyclohexane (C_6H_{12}) adsorbed on Cu(111) confirm the picture of a balance between attractive dispersion forces and a repulsive Pauli barrier. In addition, some polarisation was noticed. A strong electron sharing between the adsorbate and metal surface was found for the adsorption of octane on Cu(110) and Ni(110) [46]. Here the position of the metal *d* band with respect to the energy of the hybrid molecular–metal states was found to be important for the bond strength. It should be mentioned, however, that the calculations in [46] to some extent rest on experimental input data – a comparison between calculated and simulated X-ray adsorption spectra – and are therefore not ab initio in a strict sense.

The interaction of larger and more complex organic molecules with metal surfaces gives rise to fascinating phenomena of molecular recognition and self-assembly (see e.g. Fig. 2) that are basically not understood. Already the interaction of single polyfunctional molecules with metal substrates raises a number of interesting questions. The complex interplay and mutual influence between the surface–molecule bonds and intramolecular bonds found already for simple hydrocarbons adsorbed on metals may be substantially enhanced by the existence of various functional groups [47–51]. Nevertheless, using the adsorption of adenine on Cu(110) as an example, Preuss et al. [52] have recently shown that at least in this case the interaction of a polyfunctional molecule with a metal substrate can seemingly be rationalised in a simple and intuitive picture. The adsorption of adenine on Cu(110) is well characterised by STM, low-energy electron diffraction, electron energy-loss spectroscopy as well as cluster calculations and serves as a case study for enantiomeric interactions on solid surfaces [10, 11].

The full geometry optimisation starting with the adenine molecule (Fig. 8a) lying flat above the Cu(110) surface with a vertical distance of 2.0 Å results in the structure schematically shown in Fig. 8b. The potential energy surface (PES, Fig. 8c) shows significant structures. For adenine the copper rows are separated by an energy barrier of about 0.5 eV, and the most favourable bonding position is reached when the amino-group nitrogen is directly above a copper atom. The N–Cu bonding direction has an off-axis angle of 2.9° with respect to the surface normal.

From Fig. 8b it can also be seen that the adsorbed adenine molecule in equilibrium position is noticeably deformed with respect to its nearly planar gas-phase structure [53, 54]. Upon bonding to Cu(110) the molecule assumes a strongly

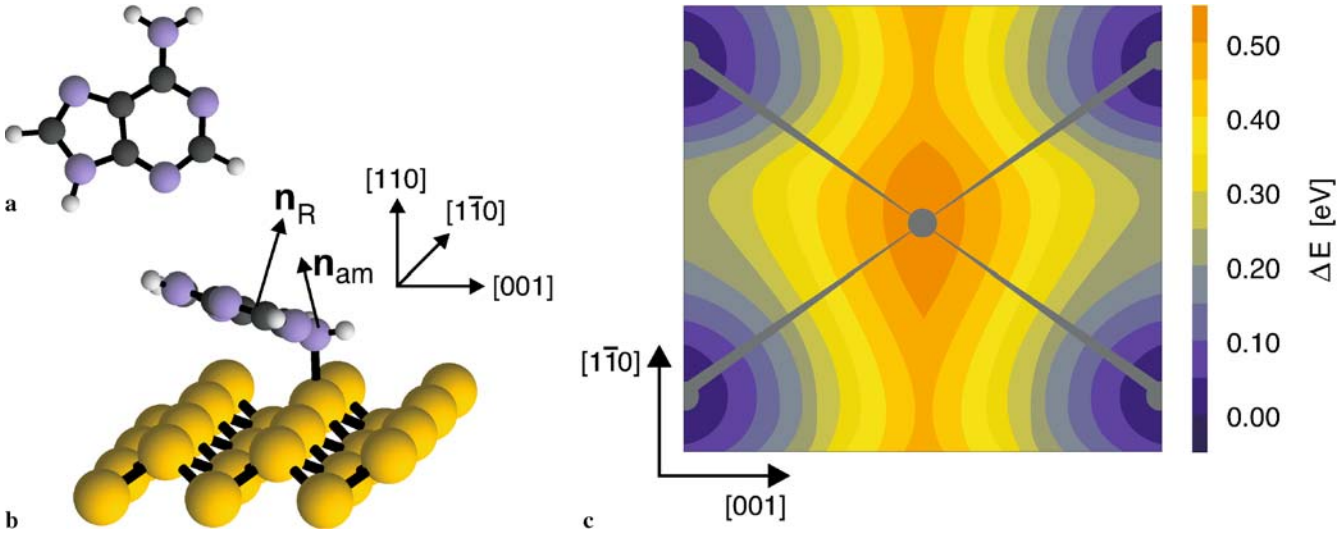

FIGURE 8 (**a**) Sketch of the adenine molecule and (**b**) the optimised adsorption geometry of adenine on Cu(110). *Blue* (*dark grey*, *light grey*, *golden*) spheres correspond to N (C, H, Cu) atoms. (**c**) The potential energy surface experienced by the adsorbed adenine molecule (*blue*/*red* indicate favourable/unfavourable adsorption sites). The Cu positions of the surface unit cell are indicated. Data from [52]

tilted geometry with the amino group NH_2 bent by 17.7° and the rest of the molecule [55] by 26.4° with respect to the surface plane. In contrast to gas-phase adenine, the amino-group nitrogen is nearly tetrahedrally coordinated with angles ranging from 112.6° to 113.4°. This is typical for sp^3 hybridised atoms. Indeed, the wave-function analysis for nitrogen indicates nearly sp^3 hybridisation ($\chi_s = 0.31$, $\chi_{p_x} = 0.23$, $\chi_{p_y} = 0.22$, $\chi_{p_z} = 0.24$). The computational results concerning the molecule tilting agree with the interpretation of vibrational spectroscopy experiments [10]. There are also small structural changes in the substrate: the Cu atom that bonds to the amino group moves out of the surface plane by 0.15 Å.

The calculated Cu–N distance of 2.32 Å is consistent with the bond lengths in organometallic Cu–N complexes [56] and slightly larger than the length of 2.10–2.13 Å reported for the respective bond of glycine adsorbed on Cu(110) [57, 58]. It certainly exceeds, however, the sum of the covalent radii of Cu and N of about 1.8 Å. Therefore, the bond is unlikely to be dominantly covalent. This is corroborated by the wave-function analysis which shows no interface orbitals with clear-cut bonding or antibonding character. Consistent with the large Cu–N distance, a relatively small adsorption energy of 0.34 eV was calculated. This seems to indicate physisorption rather than chemisorption. There are presently no experimental data available on the adsorption energy. We expect, however, the actual adsorption energy to be somewhat higher than the value calculated here: the non-locality of the van der Waals (vdW) or dispersive interaction between the electrons cannot be captured using a local functional for the exchange and correlation effects as done in the present DFT-GGA calculations. We will come back to that issue below.

Preuss et al. [52] rationalised the bonding in terms of the Coulomb interaction between molecule and substrate that are treated as virtual subsystems. The dividing plane is placed half-way between Cu and N atoms. The adsorption-induced charge redistributions within the molecule and the substrate are illustrated in Fig. 9a and b, respectively. The division of the adsystem into subsystems allows for quantifying the adsorption-induced charge transfer between molecule and substrate as well as the charge redistribution of the molecule and substrate. The electrostatic interactions between the molecule and the substrate can thus be calculated from a series of multipole terms. Since the bonding of adenine on Cu(110) is the result of a complex interplay between structural changes and charge transfer within the constituents, one also has to bear in mind the deformation energies. They reduce the energy gain due to electrostatic interactions. This has been pointed out already for various hydrocarbons adsorbed on metal substrates; see e.g. [42, 43]. In the equilibrium position it costs about $E_{\text{strain}} = 0.65\,\text{eV}$ strain energy to deform the ideal constituents into the final bonding geometry. Together with the electrostatic attraction of $E_C = -1.23\,\text{eV}$, this results in a total energy gain upon adsorption of $E_C +$

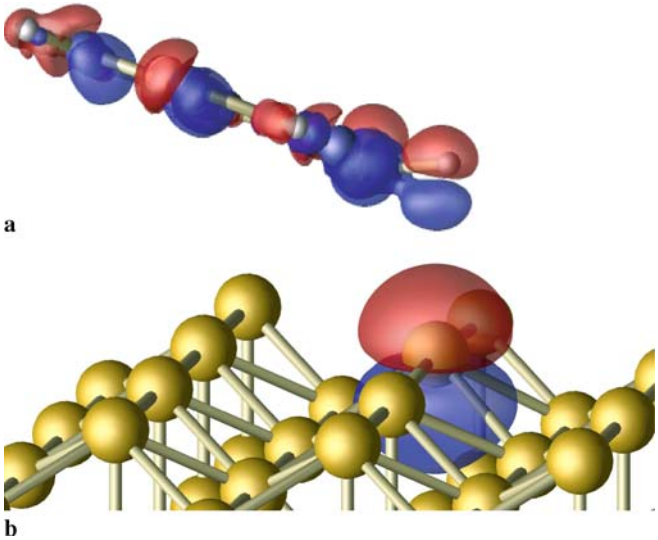

FIGURE 9 Charge-density difference with regions of electron accumulation/depletion displayed in *blue*/*red* illustrating the dipole accompanying the structural changes of the molecule (**a**) and in the substrate (**b**)

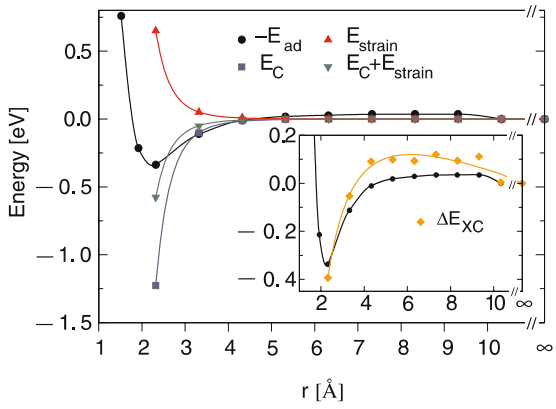

FIGURE 10 Negative adsorption energy (*circles*), strain energy (*red triangles*), Coulomb energy (*blue squares*) and sum of the latter (*green triangles pointing down*) for adenine adsorbed on Cu(110) as a function of the Cu–N distance. The *inset* shows the negative adsorption energy compared to the variation of the GGA exchange and correlation energy (*yellow diamonds*). *Solid lines* are guides to the eye. Data from [52]

$E_{\text{strain}} = -0.58$ eV. This value is of the same order of magnitude as the (negative) adsorption energy calculated from first principles.

Figure 10 shows the reaction pathway of adsorption, obtained by a series of constrained-dynamics calculations with increasing molecule–substrate distance, together with the aforementioned energy contributions. The reaction coordinate corresponds to the Cu–N distance. If the molecule approaches the surface from infinity, there is a very small energy barrier that can easily be overcome at room temperature. Starting at about 5 Å, the amino group and the metal start to polarise each other, causing an attractive potential the molecule is subject to. As seen in Fig. 10, the sum of the attractive Coulomb interaction and the energy required to deform the molecule and the substrate accounts surprisingly well for the total (negative) adsorption energy until the equilibrium bonding distance is reached. Obviously, the description of the chemical bonding in terms of such purely classical contributions cannot capture the complete physics of the interactions. This is illustrated in the inset of Fig. 10, where the difference of the GGA exchange and correlation energy relative to the isolated constituents is shown versus the bonding distance. We find a repulsive energy contribution for bonding distances larger than 3.5 Å and an attractive interaction for smaller distances. The magnitude, however, is clearly smaller than that of the Coulomb contribution discussed above. On the basis of the calculated charge-transfer characteristics the bonding can thus be explained as resulting from the combined effects of electrostatic and strain contributions. It seems very likely that the combination of attractive image forces with repulsive deformation energies is characteristic for many more organic molecules adsorbed on metal surfaces. Thus a weak bond does not imply a weak interaction, but a small resulting net energy gain, as also discussed by Nilsson and Pettersson [43].

4 Adsorption on inert surfaces

Due to the very weak, mainly dispersive, interactions between admolecules and substrate, molecular adsorption on inert surfaces provides an excellent model to probe single molecules and intermolecular interactions. On the other hand, the accurate description of the molecule–substrate interactions is particularly challenging in this case. Charge transfer and chemical bonds are, in most cases, well described within DFT with either the local-density approximation (LDA) or the GGA to account for the exchange and correlation (XC) energy of the electrons. This does not hold for dispersion or van der Waals (vdW) forces. Local (LDA) or semilocal XC functionals (GGA) fail to correctly describe the non-classical electronic interactions across regions of very sparse electron densities [59, 60]. Such regions between, for example, molecular layers and graphene sheets, enhance the relative importance of vdW coupling for the adsorption. Its calculation from first principles requires the self-consistent evaluation of the screening [61, 62], which – due to its non-locality and energy dependence – exceeds the limits of what can presently be handled numerically for complex systems, despite encouraging attempts to employ models for the screening response [60, 63].

In order to study molecular adsorption on inert surfaces computationally, a numerically tractable approach to estimate the impact of dispersive interactions needs to be devised. Ortmann et al. [64] implemented a modified London dispersion formula [65] to account for the vdW forces in DFT-GGA calculations and applied this methodology to the adsorption of adenine on graphite(0001) [6]. The adsorption of adenine on graphite has been intensively investigated in the context of the origin of life research: the self-assembly of DNA bases on template surfaces is assumed to play an essential role for the emergence of life under prebiotic conditions [66].

The London dispersion formula [65]

$$E_{ij}^{\text{vdW}}(r) = -\frac{3}{2r^6}\frac{\alpha_i \alpha_j I_i I_j}{I_i + I_j} \tag{5}$$

approximates the vdW interaction within pairs of atomic constituents i, j from their respective polarisabilities α and ionisation energies I for large atomic distances r. In order to avoid the r^{-6} singularity, and because the short-range correlations are already contained in the GGA, Ortmann et al. [64] quenched the interaction for distances below the sum of the covalent radii r_{ij} of atoms i and j by using a cutoff function

$$f(r) = 1 - \exp\left[-\lambda\left(\frac{r}{r_{ij}}\right)^8\right]. \tag{6}$$

The above description of the vdW interaction contains a single fit parameter λ. This parameter is obtained once from the requirement that $f(r)E_{ij}^{\text{vdW}}(r)$ leads to the measured graphite c lattice constant, see Fig. 11. Graphite is a prominent example highlighting the failure of GGA and LDA to account for dispersive interactions. Its structural properties are fortuitously well described within LDA, even if the interlayer binding energy is underestimated [67]. This underestimation becomes critical within GGA that fails to account for the interlayer binding [60, 68], see Fig. 11. The bonding between the graphene sheets, however, is recovered when the vdW interaction according to (5) and (6) is added to the XC energy within the GGA, yielding a longitudinal optical phonon mode

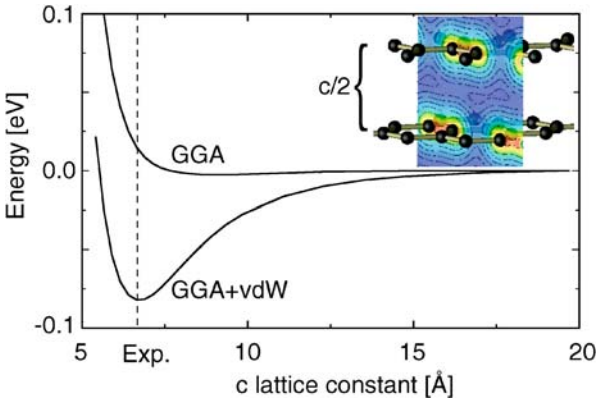

FIGURE 11 Bonding energy of graphene sheets in graphite calculated within GGA and within GGA + vdW according to (5) and (6) for varying sheet separations. The *inset* illustrates the rapid decay of the valence charge density between the sheets as calculated with DFT-GGA. *Contours* are logarithmically spaced from 2^1 to 2^{-5} Å^{-3}

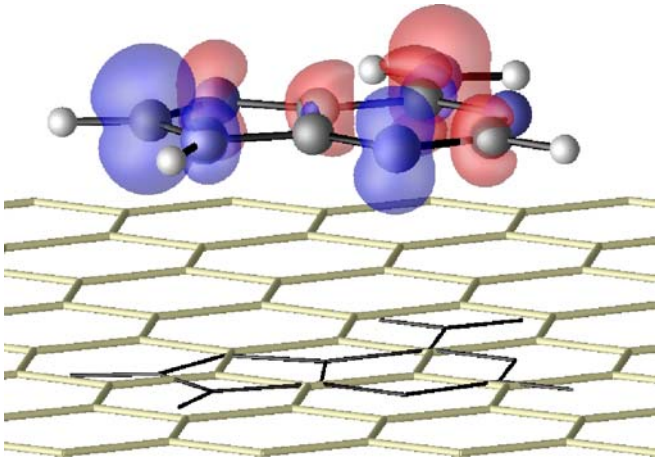

FIGURE 12 Calculated electron density changes upon adenine adsorption on graphite. Isodensity surfaces for electron gain/loss of $\pm 2 \times 10^{-5}$ Å^{-3} are shown in *blue*/*red*. Data from [6]

parallel to the [0001] direction with a frequency of 17.0 meV, close to the experimental value of 15.6 meV [69]. Ortmann et al. applied this simple scheme to a wide range of solids and molecular systems with covalent, heteropolar and vdW bonds [64]. These tests suggest the London dispersion formula as a simple, but reasonably accurate tool to supplement the GGA in systems that can be considered to be assembled from single polarisable entities for interaction distances that are clearly beyond covalent-bond lengths. Similar approximations were proposed by other authors; see e.g. [67, 70].

The corrugation of the PES experienced by adenine adsorbed on graphite is small, but depends strongly on the modelling of the dispersive forces: maximum values of 0.08 and 0.01 eV are obtained within GGA + vdW and GGA, respectively. In the ground state, the molecule adapts a planar geometry, parallel to the graphite surface. The deviations of the molecular structure from the gas-phase geometry [53] are negligible. The lateral position of the pyrimidine ring of adsorbed adenine is reminiscent of Bernal's AB stacking of graphite (see inset of Fig. 15). The lateral position of the molecule does not depend on the choice of the XC functional; there is, however, a significant influence on the vertical position. The substrate–molecule separation amounts to 3.4 and 4.0 Å within GGA + vdW and GGA, respectively. Atomic force microscopy [71] found the thickness of adenine monolayers on graphite to be about 3 Å, i.e. close to the GGA + vdW result. The adsorption energy is 1.09 and 0.07 eV within GGA + vdW and GGA, respectively. Again, the GGA + vdW value is close to the energy of 1.01 eV extracted from thermal desorption spectroscopy [72].

The adsorption energy is of similar magnitude as discussed above for adenine adsorbed on Cu(110). In this case, the adsorption was traced back to the mutual polarisation of molecule and substrate. As shown in Fig. 12, the adsorption also causes some charge redistribution in the present case. However, the electron transfer is three orders of magnitude smaller than for adenine on copper. Since the orbitals of the heterocyclic molecule are more easily polarised than the delocalised graphite electronic states, the charge redistribution mainly occurs within the molecule. Moreover, it basically occurs within the molecular plane, i.e. it does not lead to a net force along the surface normal. For that reason the mutual polarisation of molecule and graphite makes no noticeable contribution to the molecule–surface attraction.

Are weak covalent interactions responsible for the adenine–graphene bonding? We compared the orbital energies of adsorbed and gas-phase molecules. Indeed, we find some instances of small energy shifts. The most pronounced example is shown in Fig. 13: the molecular and graphite π orbitals about 7 eV below the graphite Fermi energy rehybridise to form the bonding and antibonding combinations shown in Fig. 14. The rehybridisation-related charge-density changes are extremely small. This is also reflected in the small energy changes of the orbitals. The splitting amounts to 0.3 eV only. Moreover, because both bonding and antibonding combinations are occupied, the rehybridisation does not lead to an energy gain. Rather, it acts as a repulsive Pauli barrier.

What causes the attractive molecule–substrate interaction despite a vanishing ionic contribution and a repulsive Pauli barrier? For adenine adsorbed on Cu, the XC effects in the electronic system were found to lower the adsystem energy by nearly 0.4 eV compared to the isolated systems, see Fig. 10. In that case it is only a minor contribution to the bonding. In order to study the influence of similar effects for adenine adsorbed on graphite, the XC energy for the isolated and bonded systems for different molecule–graphene distances was calculated. Indeed, a distinctly stabilising effect due to the XC energy of the inhomogeneous electron gas within the GGA and the GGA + vdW is observed, see Fig. 15. Moreover, the total bonding energy for distances beyond the equilibrium bonding distance, where the Pauli barrier becomes noticeable, follows remarkably closely the XC energy of the adenine–graphene electron gas in the GGA + vdW case. A close inspection of the XC and total-energy curves in Fig. 15 shows, however, that the XC energy is not the only cause of attraction: somewhat beyond the equilibrium bonding distances, the relative GGA/GGA + vdW XC energy is higher than the corresponding relative total energy. Analysing the remaining contributions to the energy functional shows that the kinetic energy calculated from the single-particle Kohn–Sham orbitals of the adsystem is lower than that of non-interacting adenine and graphene, due to the delocalisation of the elec-

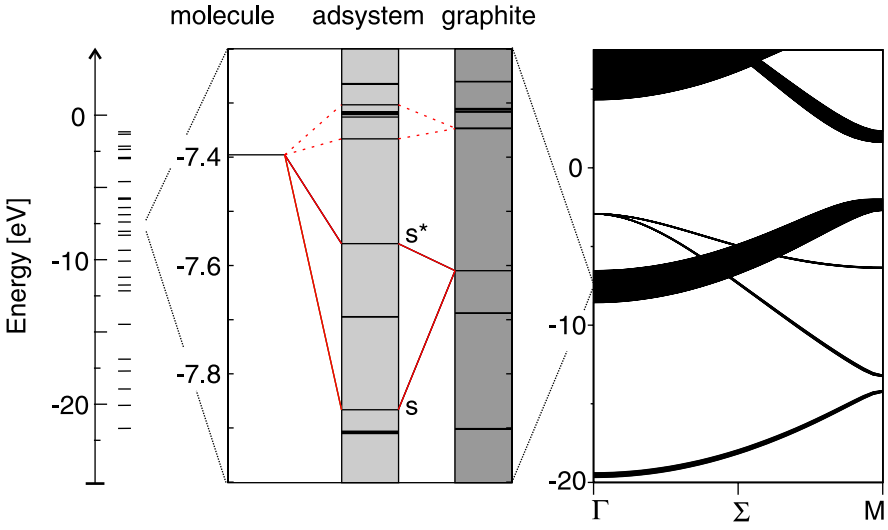

FIGURE 13 Calculated molecular energy levels of gas-phase adenine (*left*), the graphite surface projected bulk band structure (*right*) and selected energy levels of the adsorbed molecule (*middle*). Data from [6]

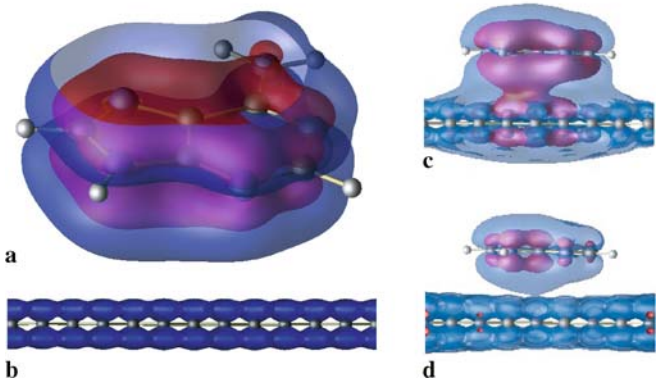

FIGURE 14 Isodensity surfaces illustrating (**a**) the molecular (*blue*/*red* $10^{-6/-5}$ Å^{-3}) and (**b**) graphite π states (10^{-6} Å^{-3}) that hybridise to form the (**c**) bonding and (**d**) antibonding combinations s and s^*, respectively (*blue*/*red* $10^{-6/-5}$ Å^{-3}). See Fig. 13

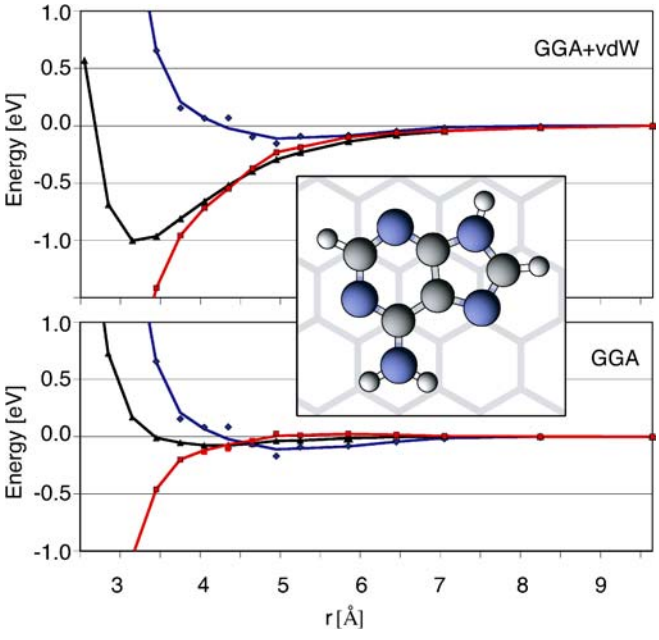

FIGURE 15 Relative total (*black triangles*), XC (*red squares*) and kinetic energy (of the Kohn–Sham particles; *blue diamonds*) of adenine adsorbed on graphene calculated as a function of the molecule–surface distance. The *inset* shows the lateral equilibrium position of adenine on graphite. Data from [6]

tronic wave functions. For distances around the respective equilibrium bonding position, however, electron XC effects are clearly responsible for the attraction: the kinetic energy of the valence electrons behaves repulsively.

While dispersive forces are obviously the dominant cause of adsorption for adenine adsorbed on graphite, they may also play an important role in instances of molecular adsorption where chemical interactions dominate: the magnitude of the vdW coupling calculated above is suitable to explain, for example, the discrepancy between the calculated small adsorption energy for adenine adsorbed on Cu(110) (see Sect. 3) and the thermal stability of this adsystem [11].

5 Conclusions and outlook

Using a few prototypical examples, some important aspects of molecule interactions with solid substrates were highlighted in this brief review.

A variety of surface reactions like nucleophilic/electrophilic, pericyclic and dissociative bonding schemes may occur during organic reactions with semiconductor surfaces. Often they pass through a dative-bonded precursor state. The diversity of these reactions is determined by thermodynamics and kinetics. It allows – in conjunction with the large variety of properties that can be realised with tailor-made molecules – for tuning the semiconductor surface functionality over an extremely wide range. This requires us, however, to accurately control competition and selectivity in the surface reactions. In addition, the structural and electronic properties of surface-bonded molecules may deviate substantially from their behaviour in gas phase.

In addition to covalent attachment schemes, mutual polarisation and image forces play a decisive role for the attachment of organic molecules to metal surfaces. Even in the absence of covalent interactions, strong charge redistribution within the molecule accompanied by structural distortions and charge transfer across the interface can occur. Thus, a weak bonding does not necessarily imply a weak interaction, but may as well result from a subtle balance between bonding forces and repulsive strain interactions.

Dispersive forces between organic molecules and chemically inert surfaces can lead to relatively large adsorption energies in excess of 1 eV. Combined with the repulsive Pauli interaction between substrate and molecule, energy barriers of up to one-tenth of an eV may hinder the lateral movement of the molecules. This comes close to the strength of intermolecular hydrogen bonds. There is thus a noticeable influence of the substrate on the molecular mobility. This needs to be taken into account when one extracts molecular interaction parameters from surface-adsorbed species.

The examples discussed here – the adsorption of uracil and phenanthrenequinone on Si(001) as well as the adsorption of adenine on copper and graphite – show the large amount of detailed information about the substrate–molecule interaction that can nowadays be obtained from first-principles calculations. The unveiling of this information, however, is only the first step towards understanding and predicting the complex and multifarious interplay of forces leading to such beautiful structures as shown in Fig. 2.

ACKNOWLEDGEMENTS Generous grants of computer time from the Höchstleistungsrechenzentrum Stuttgart (HLRS), the Leibniz-Rechenzentrum München (HLRB) and the Paderborn Center for Parallel Computing (PC^2) are gratefully acknowledged. We thank the Deutsche Forschungsgemeinschaft for financial support (grant SCHM-1361/6).

REFERENCES

1 C. Joachim, M.A. Ratner, Proc. Nat. Acad. Sci. USA **102**, 8801 (2005)
2 R. Moosbühler, G. Bayreuther, Phys. Rev. Lett. **86**, 672 (2001)
3 A. Kühnle, T.R. Linderoth, B. Hammer, F. Besenbacher, Nature **415**, 891 (2002)
4 J.V. Barth, J. Weckesser, C. Cai, P. Günter, L. Bürgi, O. Jeandupeux, K. Kern, Angew. Chem. Int. Edit. **39**, 1230 (2000)
5 O. Marchenko, J. Cousty, Phys. Rev. Lett. **84**, 5363 (2000)
6 F. Ortmann, W.G. Schmidt, F. Bechstedt, Phys. Rev. Lett. **95**, 186 101 (2005)
7 M. Furukawa, H. Tanaka, T. Kawai, Surf. Sci. **392**, L33 (1997)
8 M. Furukawa, H. Tanaka, T. Kawai, Surf. Sci. **445**, 1 (2000)
9 M. Furukawa, H. Tanaka, K. Sugiura, Y. Sakata, T. Kawai, Surf. Sci. **445**, L58 (2000)
10 Q. Chen, D.F. Frankel, N.V. Richardson, Langmuir **18**, 3219 (2002)
11 Q. Chen, N.V. Richardson, Nat. Mater. **2**, 324 (2003)
12 S.F. Bent, J. Phys. Chem. B **106**, 2830 (2002)
13 S.F. Bent, Surf. Sci. **500**, 879 (2002)
14 J.S. Hovis, H. Liu, R.J. Hamers, Appl. Phys. A **66**, S553 (1998)
15 R.J. Hamers, Nature **412**, 489 (2001)
16 M.A. Filler, S.F. Bent, Prog. Surf. Sci. **73**, 1 (2003)
17 J.-H. Cho, L. Kleinman, Phys. Rev. B **64**, 235 420 (2001)
18 W. Lu, W.G. Schmidt, J. Bernholc, Phys. Rev. B **68**, 115 327 (2003)
19 K. Seino, W.G. Schmidt, J. Furthmüller, F. Bechstedt, Phys. Rev. B **66**, 235 323 (2002)
20 K. Seino, W.G. Schmidt, Surf. Sci. **585**, 191 (2005)
21 C.A. Hacker, R.J. Hamers, J. Phys. Chem. B **107**, 7689 (2003)
22 A. Hermann, W.G. Schmidt, F. Bechstedt, J. Phys. Chem. B **109**, 7928 (2005)
23 R. Konecny, D.J. Doren, J. Chem. Phys. **106**, 2426 (1997)
24 K. Seino, W.G. Schmidt, Surf. Sci. **571**, 157 (2004)
25 B.B. Stefanov, K. Raghavachari, Appl. Phys. Lett. **73**, 824 (1998)
26 K. Seino, W.G. Schmidt, Surf. Sci. **548**, 183 (2004)
27 K. Seino, W.G. Schmidt, F. Bechstedt, Phys. Rev. B **69**, 245 309 (2004)
28 A. Lopez, Q. Chen, N. Richardson, Surf. Interf. Anal. **33**, 441 (2002)
29 K. Seino, W.G. Schmidt, M. Preuss, F. Bechstedt, J. Phys. Chem. B **107**, 5031 (2003)
30 J. Dabrowski, H.-J. Müssig, *Silicon Surfaces and Formation of Interfaces* (World Scientific, Singapore, 2000)
31 F. Bechstedt, in *Festköperprobleme/Advances in Solid State Physics*, vol. 32, ed. by U. Rössler (Vieweg, Braunschweig/Wiesbaden, 1992), p. 161
32 M. Schlüter, J.R. Chelikowsky, S.G. Louie, M.L. Cohen, Phys. Rev. B **12**, 4200 (1975)
33 W.G. Schmidt, F. Bechstedt, G.P. Srivastava, Surf. Sci. Rep. **25**, 141 (1996)
34 W. Mönch, *Semiconductor Surfaces and Interfaces* (Springer, Berlin, 1995)
35 C. Hogan, D. Paget, Y. Garreau, M. Sauvage, G. Onida, L. Reining, P. Chiaradia, V. Corradini, Phys. Rev. B **68**, 205 313 (2003)
36 S.X. Tian, C.F. Zhang, Z.J. Zhang, X.J. Chen, K.Z. Xu, Chem. Phys. **242**, 217 (1999)
37 L. Fang, J. Liu, S. Coulter, X. Cao, M.P. Schwartz, C. Hacker, R.J. Hamers, Surf. Sci. **514**, 362 (2002)
38 A. Hermann, W.G. Schmidt, F. Bechstedt, Phys. Rev. B **71**, 153 311 (2005)
39 N.A. Besley, A.J. Blundy, J. Phys. Chem. **110**, 1701 (2006)
40 M.J.S. Dewar, Bull. Soc. Chim. Fr. **18**, 79 (1951)
41 J. Chatt, L.A. Duncanson, J. Chem. Soc. 2939 (1953)
42 L. Triguero, L.G.M. Pettersson, B. Minaev, H. Ågren, J. Chem. Phys. **108**, 1193 (1998)
43 A. Nilsson, L.G.M. Pettersson, Surf. Sci. Rep. **55**, 49 (2004)
44 C. Wöll, K. Weiss, P.S. Bagus, Chem. Phys. Lett. **332**, 553 (2000)
45 P.S. Bagus, K. Hermann, C. Wöll, J. Chem. Phys. **123**, 184 109 (2005)
46 H. Öström, L. Triguero, M. Nyberg, H. Ogasawara, L.G.M. Pettersson, A. Nilsson, Phys. Rev. Lett. **91**, 046 102 (2003)
47 M. Eremtchenko, J.A. Schaefer, F.S. Tautz, Nature **425**, 602 (2003)
48 R. Di Felice, A. Selloni, E. Molinari, J. Phys. Chem. B **107**, 1151 (2004)
49 A. Ferretti, R. Di Felice, Phys. Rev. B **70**, 115 412 (2004)
50 A. Hauschild, K. Karki, B. Cowie, M. Rohlfing, F. Tautz, M. Sokolowski, Phys. Rev. Lett. **94**, 036 106 (2005)
51 A. Hauschild, K. Karki, B. Cowie, M. Rohlfing, F. Tautz, M. Sokolowski, Phys. Rev. Lett. **95**, 209 602 (2005)
52 M. Preuss, W.G. Schmidt, F. Bechstedt, Phys. Rev. Lett. **94**, 236 102 (2005)
53 M. Preuss, W.G. Schmidt, K. Seino, J. Furthmüller, F. Bechstedt, J. Comput. Chem. **25**, 112 (2004)
54 P. Pulay, S. Saebo, M. Malagoli, J. Baker, J. Comput. Chem. **26**, 599 (2005)
55 The molecule's atoms without the two hydrogen atoms of the amino group are fitted to a plane in the least-squares sense (rms = 0.03 Å) to obtain the normal vector with which the angle to the surface plane is defined. Perpendicular distances of the hydrogen atoms to this plane amount to 0.40 Å and 0.38 Å
56 T. Balasubramanian, P.T. Muthiah, A. Saravanan, S.K. Mazumdar, J. Inorg. Biochem. **63**, 175 (1996)
57 J. Hasselström, O. Karis, M. Weinelt, N. Wassdahl, A. Nilsson, M. Nyberg, L.G.M. Pettersson, M.G. Samant, J. Stöhr, Surf. Sci. **407**, 221 (1998)
58 N. Nyberg, J. Hasselström, O. Karis, N. Wassdahl, M. Weinelt, A. Nilsson, L.G.M. Pettersson, J. Chem. Phys. **112**, 5420 (2000)
59 O.A. von Lilienfeld, I. Tavernelli, U. Rothlisberger, D. Sebastiani, Phys. Rev. Lett. **93**, 153 004 (2004)
60 H. Rydberg, M. Dion, N. Jacobson, E. Schröder, P. Hyldgaard, S. Simak, D. Langreth, B. Lundqvist, Phys. Rev. Lett. **91**, 126 402 (2003)
61 J.F. Dobson, B.P. Dinte, Phys. Rev. Lett. **76**, 1780 (1996)
62 J.F. Dobson, J. Wang, Phys. Rev. Lett. **82**, 2123 (1999)
63 D.C. Langreth, M. Dion, H. Rydberg, E. Schröder, P. Hyldgaard, B.I. Lundqvist, Int. J. Quantum Chem. **101**, 599 (2005)
64 F. Ortmann, F. Bechstedt, W.G. Schmidt, Phys. Rev. B **73**, 205 101 (2006)
65 F. London, Z. Phys. Chem. B **11**, 222 (1930)
66 S.J. Sowerby, P.A. Stockwell, W.M. Heckl, G.B. Petersen, Orig. Life Evol. Biosphere **30**, 81 (2000)
67 M. Hasegawa, K. Nishidate, Phys. Rev. B **70**, 205 431 (2004)
68 K.R. Kganyago, P.E. Ngoepe, Mol. Simul. **22**, 39 (1999)
69 R. Nicklow, N. Wakabayashi, H.G. Smith, Phys. Rev. B **5**, 4951 (1972)
70 M. Elstner, P. Hobza, T. Frauenheim, S. Suhai, E. Kaxiras, J. Chem. Phys. **114**, 5149 (2001)
71 N.J. Tao, Z. Shi, J. Phys. Chem. **98**, 1464 (1994)
72 J.E. Freund, Ph.D. thesis, Ludwig-Maximilians-Universität, München (1998)